



[Increasing the range accuracy of three-dimensional ghost imaging lidar using optimum slicing number method](#)

Yang Xu, Zhang Yong, Xu Lu, Yang Cheng-Hua, Wang Qiang, Liu Yue-Hao, Zhao Yuan

Citation: Chin. Phys. B . 2015, 24(12): 124202. **doi:** 10.1088/1674-1056/24/12/124202

Journal homepage: <http://cpb.iphy.ac.cn>; <http://iopscience.iop.org/cpb>

What follows is a list of articles you may be interested in

[Ghost imaging with broad distance](#)

Duan De-Yang, Zhang Lu, Du Shao-Jiang, Xia Yun-Jie

Chin. Phys. B . 2015, 24(10): 104203. **doi:** 10.1088/1674-1056/24/10/104203

[Phase modulation pseudocolor encoding ghost imaging](#)

Duan De-Yang, Zhang Lu, Du Shao-Jiang, Xia Yun-Jie

Chin. Phys. B . 2015, 24(2): 024202. **doi:** 10.1088/1674-1056/24/2/024202

[Correspondence normalized ghost imaging on compressive sensing](#)

Zhao Sheng-Mei, Zhuang Peng

Chin. Phys. B . 2014, 23(5): 054203. **doi:** 10.1088/1674-1056/23/5/054203

[Noise analysis in ghost imaging from the perspective of coherent-mode representation](#)

Bai Yan-Feng, Yang Wen-Xing, Yu Xiao-Qiang

Chin. Phys. B . 2012, 21(4): 044206. **doi:** 10.1088/1674-1056/21/4/044206

JUST FOR AUTHOR
— CHINESE PHYSICS B

中国物理 **B**
**Chinese
Physics B**

Volume 24 Number 12 December 2015

Formerly *Chinese Physics*

A Series Journal of the Chinese Physical Society
Distributed by IOP Publishing

Online: iopscience.iop.org/cpb
cpb.iphy.ac.cn

CHINESE PHYSICAL SOCIETY
IOP Publishing |

Chinese Physics B (First published in 1992)

Published monthly in hard copy by the Chinese Physical Society and online by IOP Publishing, Temple Circus, Temple Way, Bristol BS1 6HG, UK

Institutional subscription information: 2015 volume

For all countries, except the United States, Canada and Central and South America, the subscription rate per annual volume is UK£974 (electronic only) or UK£1063 (print + electronic).

Delivery is by air-speeded mail from the United Kingdom.

Orders to:

Journals Subscription Fulfilment, IOP Publishing, Temple Circus, Temple Way, Bristol BS1 6HG, UK
For the United States, Canada and Central and South America, the subscription rate per annual volume is US\$1925 (electronic only) or US\$2100 (print + electronic). Delivery is by transatlantic airfreight and onward mailing.

Orders to:

IOP Publishing, P. O. Box 320, Congers, NY 10920-0320, USA

© 2015 Chinese Physical Society and IOP Publishing Ltd

All rights reserved. No part of this publication may be reproduced, stored in a retrieval system, or transmitted in any form or by any means, electronic, mechanical, photocopying, recording or otherwise, without the prior written permission of the copyright owner.

Supported by the National Natural Science Foundation of China, the China Association for Science and Technology, and the Science Publication Foundation, Chinese Academy of Sciences

Editorial Office: Institute of Physics, Chinese Academy of Sciences, P. O. Box 603, Beijing 100190, China

Tel: (86-10) 82649026 or 82649519, Fax: (86-10) 82649027, E-mail: cpb@aphy.iphy.ac.cn

主管单位: 中国科学院

国际统一刊号: ISSN 1674-1056

主办单位: 中国物理学会和中国科学院物理研究所

国内统一刊号: CN 11-5639/O4

承办单位: 中国科学院物理研究所

编辑部地址: 北京 中关村 中国科学院物理研究所内

主 编: 欧阳钟灿

通 讯 地 址: 100190 北京 603 信箱

出 版: 中国物理学会

Chinese Physics B 编辑部

印刷装订: 北京科信印刷厂

电 话: (010) 82649026, 82649519

编 辑: Chinese Physics B 编辑部

传 真: (010) 82649027

国内发行: Chinese Physics B 出版发行部

“Chinese Physics B”网址:

国外发行: IOP Publishing Ltd

<http://cpb.iphy.ac.cn> (编辑部)

发行范围: 公开发行

<http://iopscience.iop.org/cpb> (IOPP)

Published by the Chinese Physical Society

顾问 Advisory Board

| | | |
|-----|----------------------------------|--|
| 陈佳洱 | 教授, 院士 北京大学物理学院, 北京 100871 | Prof. Academician Chen Jia-Er School of Physics, Peking University, Beijing 100871, China |
| 冯 端 | 教授, 院士 南京大学物理系, 南京 210093 | Prof. Academician Feng Duan Department of Physics, Nanjing University, Nanjing 210093, China |
| 李政道 | 教授, 院士 | Prof. Academician T. D. Lee Department of Physics, Columbia University, New York, NY 10027, USA |
| 李荫远 | 研究员, 院士 中国科学院物理研究所, 北京 100190 | Prof. Academician Li Yin-Yuan Institute of Physics, Chinese Academy of Sciences, Beijing 100190, China |
| 丁肇中 | 教授, 院士 | Prof. Academician Samuel C. C. Ting LEP3, CERN, CH-1211, Geneva 23, Switzerland |
| 杨振宁 | 教授, 院士 | Prof. Academician C. N. Yang Institute for Theoretical Physics, State University of New York, USA |
| 杨福家 | 教授, 院士 复旦大学物理二系, 上海 200433 | Prof. Academician Yang Fu-Jia Department of Nuclear Physics, Fudan University, Shanghai 200433, China |
| 周光召 | 研究员, 院士 中国科学技术协会, 北京 100863 | Prof. Academician Zhou Guang-Zhao (Chou Kuang-Chao) China Association for Science and Technology, Beijing 100863, China |
| 王乃彦 | 研究员, 院士 中国原子能科学研究院, 北京 102413 | Prof. Academician Wang Nai-Yan China Institute of Atomic Energy, Beijing 102413, China |
| 梁敬魁 | 研究员, 院士 中国科学院物理研究所, 北京 100190 | Prof. Academician Liang Jing-Kui Institute of Physics, Chinese Academy of Sciences, Beijing 100190, China |

2012-2015

主 编 Editor-in-Chief

欧阳钟灿 研究员, 院士
中国科学院理论物理研究所,
北京 100190

Prof. Academician Ouyang Zhong-Can
Institute of Theoretical Physics, Chinese Academy of Sciences,
Beijing 100190, China

副主编 Associate Editors

赵忠贤 研究员, 院士
中国科学院物理研究所, 北京 100190
杨国桢 研究员, 院士
中国科学院物理研究所, 北京 100190
张 杰 研究员, 院士
上海交通大学物理与天文系,
上海 200240

Prof. Academician Zhao Zhong-Xian
Institute of Physics, Chinese Academy of Sciences, Beijing 100190, China
Prof. Academician Yang Guo-Zhen
Institute of Physics, Chinese Academy of Sciences, Beijing 100190, China
Prof. Academician Zhang Jie
Department of Physics and Astronomy, Shanghai Jiao Tong University,
Shanghai 200240, China

邢定钰 教授, 院士
南京大学物理学院, 南京 210093
沈保根 研究员, 院士
中国科学院物理研究所, 北京 100190
龚旗煌 教授, 院士
北京大学物理学院, 北京 100871
沈平 教授
香港科技大学物理学系, 香港九龍

编辑委员 Editorial Board

2011–2016

Prof. F. R. de Boer

Prof. H. F. Braun

陈东敏 教授

冯世平

教授
北京师范大学物理系, 北京 100875

高鸿钧

研究员, 院士
中国科学院物理研究所, 北京 100190

顾长志

研究员
中国科学院物理研究所, 北京 100190

胡岗

教授
北京师范大学物理系, 北京 100875

侯建国

教授, 院士
中国科学技术大学中国科学院结构分析
重点实验室, 合肥 230026

李方华

研究员, 院士
中国科学院物理研究所, 北京 100190

闵乃本

教授, 院士
南京大学物理系, 南京 210093

聂玉昕

研究员
中国科学院物理研究所, 北京 100190

潘建伟

教授, 院士
中国科学技术大学近代物理系,
合肥 230026

沈志勋

教授

苏肇冰

研究员, 院士
中国科学院理论物理研究所,
北京 100190

孙昌璞

研究员, 院士
中国科学院理论物理研究所,
北京 100190

王思哥

研究员, 院士
北京大学物理学院, 北京 100871

夏建白

研究员, 院士
中国科学院半导体研究所,
北京 100083

洗鼎昌

研究员, 院士
中国科学院高能物理研究所,
北京 100049

向涛

研究员, 院士
中国科学院理论物理研究所,
北京 100190

谢心澄

教授
北京大学物理学院, 北京 100871

詹文龙

研究员, 院士
中国科学院, 北京 100864

朱邦芬

教授, 院士
清华大学物理系, 北京 100084

2013–2018

Prof. Antonio H. Castro Neto

Prof. Chia-Ling Chien

Prof. David Andelman

Prof. Masao Doi

Prof. Michiyoshi Tanaka

Prof. Werner A. Hofer

丁军 教授

贺贤士

研究员, 院士
北京应用物理与计算数学研究所,
北京 100088

金晓峰

教授
复旦大学物理系, 上海 200433

Prof. Academician Xing Ding-Yu
School of Physics, Nanjing University, Nanjing 210093, China

Prof. Academician Shen Bao-Gen
Institute of Physics, Chinese Academy of Sciences, Beijing 100190, China

Prof. Academician Gong Qi-Huang
School of Physics, Peking University, Beijing 100871, China

Prof. Sheng Ping
Department of Physics, The Hong Kong University of Science and Technology,
Kowloon, Hong Kong, China

van der Waals-Zeeman Institute der Universiteit van Amsterdam
Valckenierstraat 65, 1018 XE Amsterdam, **The Netherlands**
Physikalisches Institut, Universität Bayreuth, D-95440 Bayreuth, **Germany**

Prof. Dong-Min
Rowland Institute for Science, Harvard University, **USA**

Prof. Feng Shi-Ping
Department of Physics, Beijing Normal University, Beijing 100875, China

Prof. Academician Gao Hong-Jun
Institute of Physics, Chinese Academy of Sciences, Beijing 100190, China

Prof. Gu Chang-Zhi
Institute of Physics, Chinese Academy of Sciences, Beijing 100190, China

Prof. Hu Gang
Department of Physics, Beijing Normal University, Beijing 100875, China

Prof. Academician Hou Jian-Guo
Structure Research Laboratory, University of Science and Technology of
China, Hefei 230026, China

Prof. Academician Li Fang-Hua
Institute of Physics, Chinese Academy of Sciences, Beijing 100190, China

Prof. Academician Min Nai-Ben
Department of Physics, Nanjing University, Nanjing 210093, China

Prof. Nie Yu-Xin
Institute of Physics, Chinese Academy of Sciences, Beijing 100190, China

Prof. Academician Pan Jian-Wei
Department of Modern Physics, University of Science and Technology of
China, Hefei 230026, China

Prof. Shen Zhi-Xun
Stanford University, Stanford, CA 94305-4045, **USA**

Prof. Academician Su Zhao-Bing
Institute of Theoretical Physics, Chinese Academy of Sciences,
Beijing 100190, China

Prof. Academician Sun Chang-Pu
Institute of Theoretical Physics, Chinese Academy of Sciences, Beijing
100190, China

Prof. Academician Wang En-Ge
School of Physics, Peking University, Beijing 100871, China

Prof. Academician Xia Jian-Bai
Institute of Semiconductors, Chinese Academy of Sciences,
Beijing 100083, China

Prof. Academician Xian Ding-Chang
Institute of High Energy Physics, Chinese Academy of Sciences,
Beijing 100049, China

Prof. Academician Xiang Tao
Institute of Theoretical Physics, Chinese Academy of Sciences,
Beijing 100190, China

Prof. Xie Xin-Cheng
School of Physics, Peking University, Beijing 100871, China

Prof. Academician Zhan Wen-Long
Chinese Academy of Sciences, Beijing 100864, China

Prof. Academician Zhu Bang-Fen
Department of Physics, Tsinghua University, Beijing 100084, China

Physics Department, Faculty of Science, National University of Singapore,
Singapore 117546, **Singapore**

Department of Physics and Astronomy, The Johns Hopkins University,
Baltimore, MD 21218, **USA**

School of Physics and Astronomy, Tel Aviv University, Tel Aviv 69978, **Israel**

Toyota Physical and Chemical Research Institute, Yokomichi, Nagakute,
Aichi 480-1192, **Japan**

Research Institute for Scientific Measurements, Tohoku University, Katahira
2-1-1, Aoba-ku 980, Sendai, **Japan**

Stephenson Institute for Renewable Energy, The University of Liverpool,
Liverpool L69 3BX, **UK**

Prof. Ding Jun
Department of Materials Science & Engineering, National University of
Singapore, Singapore 117576, **Singapore**

Prof. Academician He Xian-Tu
Institute of Applied Physics and Computational Mathematics, Beijing 100088,
China

Prof. Jin Xiao-Feng
Department of Physics, Fudan University, Shanghai 200433, China

李儒新 研究员
中国科学院上海光学精密机械研究所,
上海 201800
吕力 研究员
中国科学院物理研究所, 北京 100190
李晓光 教授
中国科学技术大学物理系, 合肥 230026
沈元壤 教授
王亚愚 教授
清华大学物理系, 北京 100084
王玉鹏 研究员
中国科学院物理研究所, 北京 100190
王肇中 教授
闻海虎 教授
南京大学物理学院系, 南京 210093
徐至展 研究员, 院士
中国科学院上海光学精密机械研究所,
上海 201800
许岑珂 助理教授
薛其坤 教授, 院士
清华大学物理系, 北京 100084
叶军 教授

张振宇 教授

2015–2020

Prof. J. Y. Rhee
Prof. Robert J. Joynt
程建春 教授
南京大学物理学院, 南京 210093
戴希 研究员
中国科学院物理研究所, 北京 100190
郭光灿 教授, 院士
中国科学技术大学物理学院, 合
肥 230026
刘朝星 助理教授
刘荧 教授
上海交通大学物理与天文系, 上
海 200240
龙桂鲁 教授
清华大学物理系, 北京 100084
牛谦 教授
欧阳颀 教授, 院士
北京大学物理学院, 北京 100871
孙秀冬 教授
哈尔滨工业大学物理系, 哈尔滨 150001
童利民 教授
浙江大学光电信息工程学系, 杭
州 310027
童彭尔 教授
香港科技大学物理系, 香港九龍
王开友 研究员
中国科学院半导体研究所, 北京 100083
魏苏淮 教授
解思深 研究员, 院士
中国科学院物理研究所, 北京 100190
叶朝辉 研究员, 院士
中国科学院武汉物理与数学研究所,
武汉 430071
郁明阳 教授
张富春 教授
香港大学物理系, 香港
张勇 教授
郑波 教授
浙江大学物理系, 杭州 310027
周兴江 研究员
中国科学院物理研究所, 北京 100190

编辑 Editorial Staff

王久丽 Wang Jiu-Li 章志英 Zhang Zhi-Ying 蔡建伟 Cai Jian-Wei 翟振 Zhai Zhen 郭红丽 Guo Hong-Li

Prof. Li Ru-Xin
Shanghai Institute of Optics and Fine Mechanics, Chinese Academy of
Sciences, Shanghai 201800, China
Prof. Lü Li
Institute of Physics, Chinese Academy of Sciences, Beijing 100190, China
Prof. Li Xiao-Guang
Department of Physics, University of Science and Technology of China,
Hefei 230026, China
Prof. Shen Yuan-Rang
Lawrence Berkeley National Laboratory, Berkeley, CA 94720, **USA**
Prof. Wang Ya-Yu
Department of Physics, Tsinghua University, Beijing 100084, China
Prof. Wang Yu-Peng
Institute of Physics, Chinese Academy of Sciences, Beijing 100190, China
Prof. Wang Zhao-Zhong
Laboratory for Photonics and Nanostructures(LPN) CNRS-UPR20,
Route de Nozay, 91460 Marcoussis, **France**
Prof. Wen Hai-Hu
School of Physics, Nanjing University, Nanjing 210093, China
Prof. Academician Xu Zhi-Zhan
Shanghai Institute of Optics and Fine Mechanics, Chinese Academy of
Sciences, Shanghai 201800, China
Assist. Prof. Xu Cen-Ke
Department of Physics, University of California, Santa Barbara, CA 93106,
USA
Prof. Academician Xue Qi-Kun
Department of Physics, Tsinghua University, Beijing 100084, China
Prof. Ye Jun
Department of Physics, University of Colorado, Boulder,
Colorado 80309-0440, **USA**
Prof. Z. Y. Zhang
Oak Ridge National Laboratory, Oak Ridge, TN 37831–6032, **USA**

Department of Physics, Sungkyunkwan University, Suwon, **Korea**
Physics Department, University of Wisconsin-Madison, Madison, **USA**
Prof. Cheng Jian-Chun
School of Physics, Nanjing University, Nanjing 210093, China
Prof. Dai Xi
Institute of Physics, Chinese Academy of Sciences, Beijing 100190, China
Prof. Academician Guo Guang-Can
School of Physical Sciences, University of Science and Technology of China,
Hefei 230026, China
Assist. Prof. Liu Chao-Xing
Department of Physics, Pennsylvania State University PA 16802-6300, **USA**
Prof. Liu Ying
Department of Physics and Astronomy, Shanghai Jiao Tong University,
Shanghai 200240, China
Prof. Long Gui-Lu
Department of Physics, Tsinghua University, Beijing 100084 China
Prof. Niu Qian
Department of Physics, University of Texas, Austin, TX 78712, **USA**
Prof. Academician Ouyang Qi
School of Physics, Peking University, Beijing 100871, China
Prof. Sun Xiu-Dong
Department of Physics, Harbin Institute of Technology, Harbin 150001, China
Prof. Tong Li-Min
Department of Optical Engineering, Zhejiang University,
Hangzhou 310027, China
Prof. Tong Peng-Er
Department of Physics, The Hong Kong University of Science and Technology,
Kowloon, Hong Kong, China
Prof. Wang Kai-You
Institute of Semiconductors, Chinese Academy of Sciences, Beijing 100083,
China
Prof. Wei Su-Huai
National Renewable Energy Laboratory, Golden, Colorado 80401-3393, **USA**
Prof. Academician Xie Si-Shen
Institute of Physics, Chinese Academy of Sciences, Beijing 100190, China
Prof. Academician Ye Chao-Hui
Wuhan Institute of Physics and Mathematics, Chinese Academy of Sciences,
Wuhan 430071, China
Prof. Yu Ming-Yang
Theoretical Physics I, Ruhr University, D-44780 Bochum, **Germany**
Prof. Zhang Fu-Chun
Department of Physics, The University of Hong Kong, Hong Kong, China
Prof. Zhang Yong
Electrical and Computer Engineering Department, The University of North
Carolina at Charlotte, Charlotte, **USA**
Prof. Zheng Bo
Physics Department, Zhejiang University, Hangzhou 310027, China
Prof. Zhou Xing-Jiang
Institute of Physics, Chinese Academy of Sciences, Beijing 100190, China

Increasing the range accuracy of three-dimensional ghost imaging ladar using optimum slicing number method*

Yang Xu(杨旭), Zhang Yong(张勇), Xu Lu(徐璐), Yang Cheng-Hua(杨成华),
Wang Qiang(王强), Liu Yue-Hao(刘越豪), and Zhao Yuan(赵远)[†]

Department of Physics, Harbin Institute of Technology, Harbin 150001, China

(Received 28 April 2015; revised manuscript received 7 July 2015; published online 20 October 2015)

The range accuracy of three-dimensional (3D) ghost imaging is derived. Based on the derived range accuracy equation, the relationship between the slicing number and the range accuracy is analyzed and an optimum slicing number (OSN) is determined. According to the OSN, an improved 3D ghost imaging algorithm is proposed to increase the range accuracy. Experimental results indicate that the slicing number can affect the range accuracy significantly and the highest range accuracy can be achieved if the 3D ghost imaging system works with OSN.

Keywords: ghost imaging, range accuracy, optimum slicing number

PACS: 42.30.Va, 42.50.Dv

DOI: 10.1088/1674-1056/24/12/124202

1. Introduction

Ghost imaging with a thermal source has been widely studied recently.^[1–5] Moreover, Erkmen and Shapiro described a computational ghost imaging arrangement, the so-called virtual ghost imaging, by utilizing a single bucket detector with no spatial resolution.^[6,7] Their proposed method facilitated the application of ghost imaging in practice.^[8] Unlike the conventional thermal ghost imaging, their proposal omitted the reference arm path. From then on, more and more researchers have paid a great deal of attention to the application of ghost imaging.^[9–14] More recently, three-dimensional (3D) ghost imaging has been reported.^[15,16] Compared with the two-dimensional (2D) ghost imaging, 3D ghost imaging can provide a great deal of information about the target for remote sensing.

However, there is no analysis on the range accuracy of the 3D ghost imaging. Range accuracy is one of the most important parameters to evaluate the quality of range images and the centroid method is usually utilized to increase the range accuracy. In this paper, the range accuracy of 3D ghost imaging with the centroid method is derived for the first time and the influence of the slicing number on the range accuracy is also analyzed. According to the theoretical analysis, it is concluded that a large slicing number cannot always assure a high range accuracy. Therefore, an optimum slicing number (OSN) of the 3D ghost imaging is determined. The slicing number over or below the OSN will lead to the decrease of range accuracy of the 3D ghost imaging. In addition, the OSN method is introduced to increase the range accuracy and the OSN is also derived based on the range equation.

An outdoor experiment is performed in the study to il-

luminare the theoretical analysis results. The target of our experiment is a wall of a building about 180 m away. The OSN method, centroid method, and conventional method are utilized to obtain range images of the target respectively. A comparison among the range images obtained with different methods shows that the range accuracy of the OSN method is best. The range image of the target is measured by a scanning laser radar used as a reference, and range accuracies of range images obtained with different methods are calculated. The calculated results quantitatively indicate that the range accuracy with the OSN method is highest. The investigation of this study shows the potential application of 3D ghost imaging in the field of remote sensing in the future.

2. Theory of 3D ghost imaging with centroid method

The difference between conventional 2D ghost imaging and 3D ghost imaging is that the sensor with no spatial resolution (bucket detector) of 3D ghost imaging is a time-resolved detector. The reflected light from the target is collected by no spatial resolution detector. If targets are located at different positions, ghost imaging of all the different targets can be obtained at different time slices. The schematic of the 3D ghost imaging system is shown in Fig. 1. The source of this system is a pulse laser. The laser is modulated by a transmission spatial light modulator (SLM) and a telescope system is utilized to emit speckle patterns on the target. The detector in this system is a time-resolution single-pixel detector and we use a collecting lens to collect echo light. After a correlation calculation between the output of the bucket detector and speckle intensity distributions, 3D images of the target can be obtained.

*Project supported by the Young Scientist Fund of the National Natural Science Foundation of China (Grant No. 61108072).

[†]Corresponding author. E-mail: zhaoyuan@hit.edu.cn

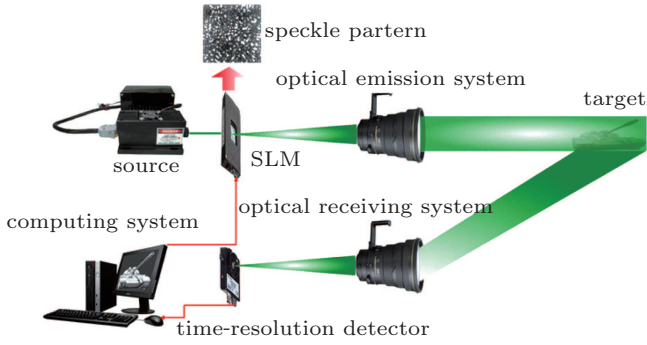


Fig. 1. (color online) Schematic diagram of 3D ghost imaging system.

According to the basic theory of ghost imaging, the image of a certain time slice can be obtained by correlating total reflected light intensity $B(t)$ measured by time-resolution single-pixel detector and the intensity distribution of speckle pattern $I(\mathbf{r}, t)$ measured by the CCD. The speckle pattern $I(\mathbf{r}, t)$ illuminating on targets is generated by computer. Hence, the correlation function of intensity fluctuations $G^{(2)}(\mathbf{r}, t)$ can be expressed as^[17]

$$G^{(2)}(\mathbf{r}, t) = \langle B_s(t) I_s(\mathbf{r}, t) \rangle - \langle B_s(t) \rangle \langle I_s(\mathbf{r}, t) \rangle. \quad (1)$$

In Eq. (1), $G^{(2)}(\mathbf{r}, t)$ presents the image of 3D ghost imaging at a certain time-slice t ; $\langle X \rangle = \frac{1}{M} \sum_s^M X_s$ represents the ensemble average, where M is the number of measurements, subscript s refers to the s -th experiment at the time slice t ; $I(\mathbf{r}, t)$ denotes the intensity distribution of the speckle pattern illuminating the target at the transverse coordinate \mathbf{r} and the time slice t . The 3D ghost imaging is used to obtain the images in the far field. Hence, the speckle patterns at different time slices are the same. It implies that the speckle pattern $I(\mathbf{r}, t)$ does not change with time slice t . Hence, $I(\mathbf{r}, t)$ can be expressed as $I(\mathbf{r})$. In Eq. (1), $B_s(t)$ is the reflective intensity in the object arm at the time slice t . $B_s(t)$ takes different values at various time slices. It is because the targets in the field of view are at different positions and the echo light beams from the different targets are not the same.

In the setup, the light of the laser is expressed as

$$P(t) = P_0 \exp \left[-\frac{t^2}{2a^2} \right], \quad (2)$$

where P_0 is the peak power of the laser and a is the pulse width. The intensity distribution of the laser is modulated by the SLM. Therefore, the intensity distribution illuminating the target can be given by

$$P(\mathbf{r}, t) = P_0 \exp \left[-\frac{t^2}{2a^2} \right] \cdot I(\mathbf{r}), \quad (3)$$

where $I(\mathbf{r})$ is the speckle pattern illuminating the target. Supposing that the optical receiving system can collect all the echo light from targets, the intensity reflected from the targets at the transverse coordinates \mathbf{r} is described as

$$R(\mathbf{r}, t) = I(\mathbf{r}) \cdot T(\mathbf{r}) P_0 \exp \left[-\frac{t^2}{2a^2} \right] g(t), \quad (4)$$

where $T(\mathbf{r})$ is the reflectivity of the target and $g(t)$ is the range-gate of the detector. In this system, the range-gate of this bucket detector is expressed as

$$g(t) = \sum_{n=1}^N \delta(t - t_1 - nT), \quad (5)$$

where t_1 is the start time, T is the time step, and N is the total number of range gates. Suppose that $t_0^{(r)}$ is the time delay of the corresponding object at the transverse coordinates \mathbf{r} . Submitting Eq. (5) into Eq. (4), the bucket detector received by gate n is given by

$$B(n) = \sum_{\mathbf{r}} I(\mathbf{r}) \cdot T(\mathbf{r}) P_0 \exp \left[-\frac{(t_0^{(r)} - t_1 - nT)^2}{2a^2} \right]. \quad (6)$$

According to Eqs. (1) and (6), the n th slice of the correlation function of intensity fluctuations is expressed as

$$G^{(2)}(\mathbf{r}, t_1 + nT) = P_0 \exp \left[-\frac{(t_0^{(r)} - t_1 - nT)^2}{2a^2} \right] G(\mathbf{r}), \quad (7)$$

$$G(\mathbf{r}) = \frac{1}{M} \sum_{n=1}^M \left(\sum_{\mathbf{r}} I(\mathbf{r}) \cdot T(\mathbf{r}) \right) \cdot I_s(\mathbf{r}) - \frac{1}{M} \sum_{n=1}^M \left(\sum_{\mathbf{r}} I(\mathbf{r}) \cdot T(\mathbf{r}) \right) \cdot \frac{1}{M} \sum_{s=1}^M I_s(\mathbf{r}), \quad (8)$$

where $G(\mathbf{r})$ is the ghost image at the transverse coordinate \mathbf{r} . The number of measurement M should be very large to ensure a high enough SNR.

Through Eqs. (7) and (8), we can obtain K slices of intensity images. For transverse coordinate \mathbf{r} , the maximum $G^{(2)}(\mathbf{r}, t_1 + nT)$ can be picked out and the corresponding n should be recorded as m . Therefore, in the conventional method, the distance between the target at transverse coordinate \mathbf{r} and the detection system can be expressed as

$$d_r = \frac{c}{2} (t_1 + mT) \quad \text{s.t.} \\ m = \arg \max \left\{ G^{(2)}(\mathbf{r}, t_1 + mT) \right\}_{m=1 \dots K}. \quad (9)$$

However, the range accuracy of this method is relatively low. In practice, the centroid method is utilized to process the ghost imaging slice.

With the help of Eq. (7), the distance at transverse coordinates \mathbf{r} can be derived by the centroid method, which can be expressed as

$$d = \frac{c}{2} \frac{\sum_{n=1}^N (t_1 + nT) \left(G(\mathbf{r}) P_0 \exp \left[-\frac{(t_0^{(r)} - t_1 - nT)^2}{2a^2} \right] \right)}{\sum_{n=1}^N \left(G(\mathbf{r}) P_0 \exp \left[-\frac{(t_0^{(r)} - t_1 - nT)^2}{2a^2} \right] \right)}. \quad (10)$$

Range accuracy is an important parameter to evaluate the quality of the 3D ghost imaging. Range accuracy $\Delta d = d - ct_0^{(r)}/2$ is given by

$$\Delta d = \frac{c}{2} \frac{\sum_{n=1}^N (t_1 + nT - t_0^{(r)}) \left(G(r) P_0 \exp \left[-\frac{(t_0^{(r)} - t_1 - nT)^2}{2a^2} \right] \right)}{\sum_{n=1}^N \left(G(r) P_0 \exp \left[-\frac{(t_0^{(r)} - t_1 - nT)^2}{2a^2} \right] \right)}. \quad (11)$$

3. Analysis of the range accuracy of 3D ghost imaging

Equation (11) gives the range accuracy of 3D ghost imaging with the centroid method. When $t_1 - t_0^{(r)} = \frac{1}{2}nT$ and the SNR of intensity images is at a high value, range accuracy Δd should be 0. In ghost imaging, the noise is always larger than the signal in a single shot measurement. Thousands of measurements are performed and averaged to obtain the high-quality intensity images. Suppose that there are M -shot measurements, the SNR of the ghost imaging is \sqrt{M} times larger than that of a single shot measurement.^[18] If the number of

measurements is large enough, the SNR can be a considerable value. Nevertheless, the number of the measurements is not infinite. The influence of the noise on the 3D ghost imaging range accuracy cannot be ignored.

When the noise of intensity images is not small enough to be ignored, the ghost image is:

$$G(r) = G'(r) \left(1 + \frac{1}{SNR_n} \right), \quad (12)$$

where $G'(r)$ is the ghost image signal, and noise of ghost imaging can be expressed as noise = $G'(r)/SNR_n$. Submitting Eq. (11) into Eq. (12), the range accuracy is given as

$$\Delta d = \frac{c}{2} \frac{\sum_{n=1}^N (t_1 + nT - t_0^{(r)}) \left(G(r) \left(1 + \frac{1}{SNR_n} \right) P_0 \exp \left[-\frac{(t_0^{(r)} - t_1 - nT)^2}{2a^2} \right] \right)}{\sum_{n=1}^N \left(G(r) \left(1 + \frac{1}{SNR_n} \right) P_0 \exp \left[-\frac{(t_0^{(r)} - t_1 - nT)^2}{2a^2} \right] \right)}. \quad (13)$$

According to Eq. (13), the range accuracy changes with the slicing number. Figure 2 shows the variations of range accuracy with the slicing number for different SNR levels. The average SNR of all slices is utilized to value the SNR level, and average SNR is expressed as

$$SNR = \frac{1}{K} \sum_{n=1}^K SNR_n, \quad (14)$$

where K is the total number of slices. In Fig. 2, the average SNR values of all slices are selected as 1, 10, 100. If SNR is at a high level, the range accuracy improves with the increase of the slicing number. When the slicing number is selected to be above a certain value, the range accuracy does not change with the slicing number. If SNR is at a low level, the range accuracy improves rapidly like the high level SNR circumstance below a

certain slicing number. However, when the slicing number is above this slicing number, the influence of the noise becomes more and more intense. Range accuracy fluctuation greatly increases with slicing number increasing. Therefore, simply increasing the slicing number will reduce the range accuracy. The slicing number should be set as a particular value to ensure a high range accuracy. This particular value is defined as the optimum slicing number (OSN) of the system.

According to the above analysis, it can be concluded that the noise is a major factor influencing the range accuracy when the slicing number is greater than the OSN. When the slicing number is less than or equal to OSN, the range accuracies at different SNR levels are nearly the same. Therefore, we can use Eq. (11) to calculate the range of targets. Range accuracy is best when the slicing number is set as OSN. We propose to process each range slice according to the OSN and to synthesize the results into a full range image. The OSN method can be expressed as

$$d = \frac{c}{2} \frac{\sum_{m-N/2}^{m+N/2} (t_1 + nT) \left(G(r) P_0 \exp \left[-\frac{(t_0^{(r)} - t_1 - nT)^2}{2a^2} \right] \right)}{\sum_{m-N/2}^{m+N/2} \left(G(r) P_0 \exp \left[-\frac{(t_0^{(r)} - t_1 - nT)^2}{2a^2} \right] \right)}, \quad (15)$$

where N is the OSN; $n = 1, 2, 3, \dots$; and $G^{(2)}(r, t_1 + nT)$ reaches the maximum value when $n = m$. Through Eq. (14),

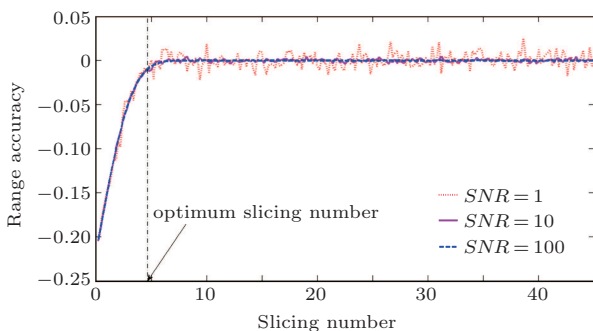


Fig. 2. (color online) Variations of range accuracy with the slicing number for average SNR values of 1, 10, and 100.

we can determine the OSN which is considered as the key point for the OSN method. According to the definition of m , the maximum of the correlation function of intensity fluctuation $G^{(2)}(\mathbf{r}, t_1 + nT)_{\max}$ is expressed as

$$G^{(2)}(\mathbf{r}, t_1 + nT)_{\max} = P_0 \exp \left[-\frac{(t_0^{(r)} - t_1 - mT)^2}{2a^2} \right] G(r). \quad (16)$$

If $G^{(2)}(\mathbf{r}, t_1 + nT)$ satisfies the inequality

$$G^{(2)}(\mathbf{r}, t_1 + nT) < \frac{G^{(2)}(\mathbf{r}, t_1 + nT)_{\max}}{SNR},$$

the contribution of the correlation function of intensity fluctuation $G^{(2)}(\mathbf{r}, t_1 + nT)$ to \mathbf{r} is less than that of the noise of $G^{(2)}(\mathbf{r}, t_1 + nT)_{\max}$. In this case, these calculated intensity fluctuations are actually unreliable and should be rejected. According to Eq. (13), when $n = m + N/2$ and $n = m - N/2$, $G^{(2)}(\mathbf{r}, t_1 + nT)$ equals $G^{(2)}(\mathbf{r}, t_1 + nT)_{\max}/SNR$. Utilizing Eqs. (7) and (15), the relationship is shown as

$$\begin{cases} \exp \left[-\frac{(t_0^{(r)} - t_1 - (m + \frac{N}{2})T)^2}{2a^2} \right] \\ = \frac{1}{SNR} \exp \left[-\frac{(t_0^{(r)} - t_1 - mT)^2}{2a^2} \right], \\ \exp \left[-\frac{(t_0^{(r)} - t_1 - (m - \frac{N}{2})T)^2}{2a^2} \right] \\ = \frac{1}{SNR} \exp \left[-\frac{(t_0^{(r)} - t_1 - mT)^2}{2a^2} \right]. \end{cases} \quad (17)$$

Solving Eq. (15), the OSN is given by

$$N = \frac{2}{T} \sqrt{2a^2 \ln SNR}. \quad (18)$$

The noise of ghost imaging originates from different combinations of field variations and shot noises.^[19,20] As to our system, SNR is dominated by the shot noise of a single pixel detector and the noise generated during the propagation of a speckle. The OSN method is a modified centroid method which can eliminate the influence of shot noise. Besides, the conventional centroid method utilizes all ghost imaging slices to calculate the range image. All the noise from slices without target information will reduce the 3D ghost imaging range accuracy. With the OSN method, only the slices containing target information are used to obtain the range image. Noises from useless slices cannot influence the range image. Therefore, the range accuracy of 3D ghost imaging with the OSN method is higher than that with the conventional method and the centroid method.

4. Experiment of 3D ghost imaging

In order to further illustrate that the OSN method can improve the range accuracy of 3D ghost imaging, the experiment is carried out.

In our experimental system, a diode-pumped, active Q-switched Nd:YAG solid-state laser is used as a source. The wavelength of the laser is at 532 nm with a pulse width of 30 ns. The repetition frequency of a pulse is 10 Hz and the average energy of each pulse is 0.2 mJ. The laser is controlled by an external triggering.

The SLM in our system is a translucent liquid crystal SLM based on the amplitude. Its maximum frame rate is 60 Hz. In this experiment, the SLM works at a frame rate of 10 Hz. The active area of the SLM is 36.9 mm × 27.6 mm and its pixel size is 32 μm × 32 μm. The SLM is controlled by a computer which generates the random binary patterns, and transmits them to the SLM. The size of the random binary pattern is 1024 × 768 and the rate of change of the pattern on the SLM is 10 Hz.

The echoed signal is recorded by an ultrafast PIN photodiode with 1.5 GHz response frequency. There is a high-speed data acquisition card connected to the PIN photodiode and the sampling frequency of this data acquisition card is 200 MHz. The data acquisition card is used to record the echoed light from the target at the different time slices. The interval between every two slices is 10ns. This experiment performs 10000-times continuous measurements to obtain the experimental results.

A 75-mm aperture convex lens with a focal length of 300 mm is utilized as the optical receiving system. There is a 5-nm narrow-band filter with a wavelength of 532-nm positioned in front of the PIN photodiode. The experiment is conducted at night, and the narrow-band filter in the experiment is used to reduce the background noise as much as possible. This experiment is performed on condition that the laser pulse width is 10 ns, the SNR is 10, and the target is about 180m away. According to Eq. (16), the OSN of our experimental system is calculated to be 4.

The experimental targets and the 3D ghost imaging results obtained respectively by the conventional method, the centroid method and the OSN method are all shown in Fig. 3. Figure 3(a) shows the picture of the target and the range of this target is from 160 m to 190 m. Figures 3(b)–3(d) are the results of 3D ghost imaging, obtained by the conventional method, the centroid method and the OSN method respectively. As shown in Fig. 3(a), the target is a wall of a building. The normal direction of the target is not parallel to the illuminating direction. Figures 3(b)–3(d) are range images of the target in a red rectangular frame in Fig. 3(a), obtained by different methods. Different colors in these range images represent different ranges. Utilizing the colorbar and colors on the range images, range information can be obtained intuitively.

Results with different methods are not similar to each other. As shown in Fig. 3(a), the range of the wall from right to

left increases gradually. Therefore, the color of range images from right to left should change from blue to red gradually. However, the color of Fig. 3(b) changes from right to left in a stepwise manner. There is an obvious boundary between different colors. The range accuracy of Fig. 3(b) is lower than that of Fig. 3(d). Although, the color of Fig. 3(c) changes gradually from right to left, there are many noise points in the

range image. The range accuracy of Fig. 3(c) is also lower than that of Fig. 3(d). Unlike the colors of Figs. 3(b) and 3(c), the color of Fig. 3(d) changes gradually from right to left, and the number of noise points is less than those in Fig. 3(c). Of all the above, the range accuracy of OSN is highest, which is shown by comparing differences between Figs. 3(a), 3(b), and 3(c).

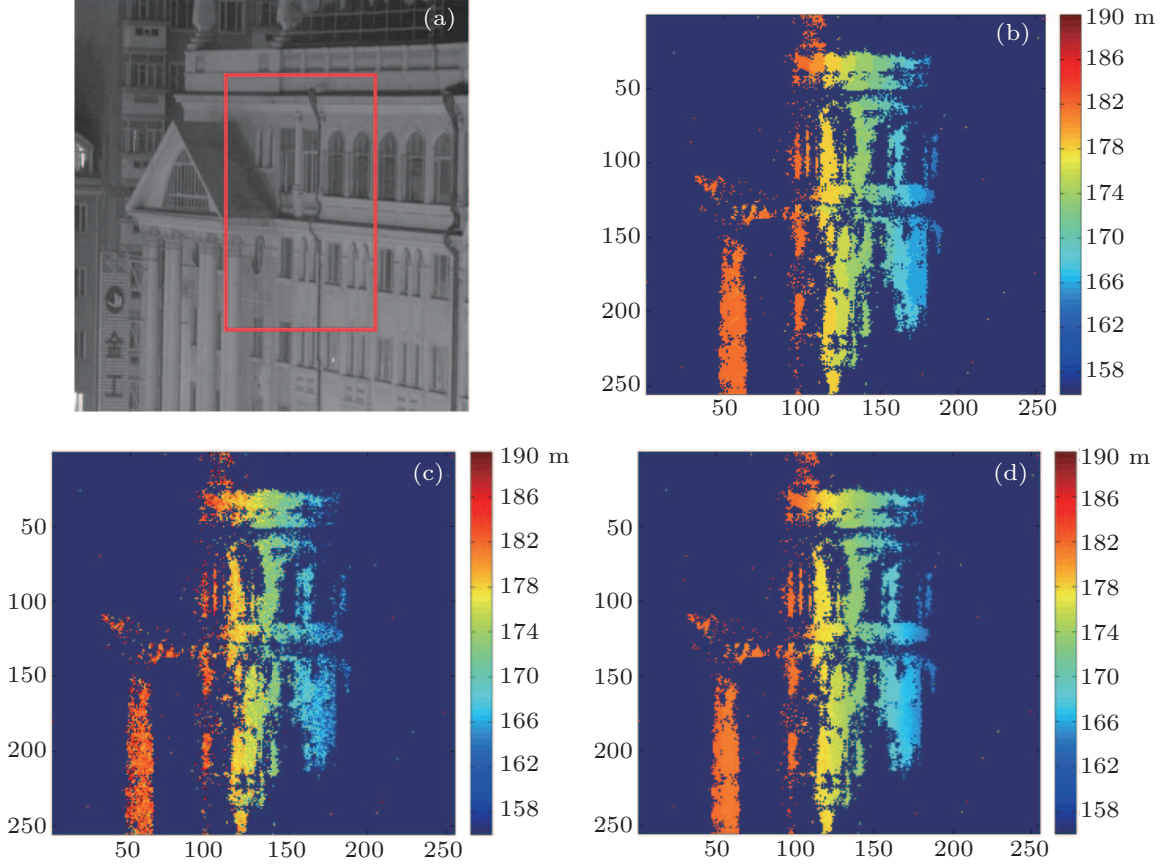


Fig. 3. (color online) (a) Picture of the target and the target about 180 m away, 3D ghost images obtained with (b) the conventional method, (c) the centroid method, and (d) the OSN method. The colorbar on the right side in each panel represents the range scale.

Furthermore, in order to illuminate that the range accuracy of Fig. 3(d) is better than those of Figs. 3(b) and 3(c) quantitatively, range accuracy values of Figs. 3(b)–3(d) are calculated respectively. We utilize the range root-mean-square error (RMSE) to evaluate the range accuracy. The RMSE is expressed as

$$\sigma = \sqrt{\sum_{i,j} \frac{(G_{i,j} - O_{i,j})^2}{i \times j}}, \quad (19)$$

where $G_{i,j}$ is the range image value of the (i, j) target, obtained with one of the above methods, and $O_{i,j}$ is the real range value of the (i, j) target. (i, j) represents the coordinate of the range image. According to Eq. (17), the RMSE of Fig. 3(b) is $\sigma_1 = 1.47$ m; the RMSE of Fig. 3(c) is $\sigma_2 = 0.94$ m; and the RMSE of Fig. 3(d) is $\sigma_3 = 0.47$ m. By comparing the RMSEs of the range image obtained with different methods, it can be

concluded that the range accuracy of Fig. 3(d) is higher than those of Figs. 3(b) and 3(c).

The experimental results and the calculated RMSEs illustrate that Fig. 3(d) accords more with the reality than Figs. 3(b) and 3(c). The range image of the target in Fig. 3(d) can correctly reflect the range information of the target. The range accuracy of Fig. 3(d) based on the OSN method is nearly a third higher than that of Fig. 3(b) obtained using the conventional method and twice higher than that of Fig. 3(c) obtained using the centroid method. The experimental results strongly support the theoretical analysis in the subsection.

5. Conclusions

In this paper, the relationship between the slicing number and the range accuracy of the 3D ghost imaging is established for different SNRs. An OSN of the 3D ghost imaging is de-

terminated in this paper. When the 3D ghost imaging system works with the OSN method, the highest range accuracy can be achieved. According to the theoretical demonstration and the experimental analysis, one can come to the conclusion that utilizing the advanced method proposed in this paper can enhance the range accuracy significantly, and provide the range information of the target effectively. This research could promote the development of 3D ghost imaging in practice.

References

- [1] Gatti A, Brambilla E and Lugiato L A 2004 *Phys. Rev. Lett.* **93** 093602
- [2] Gatti A, Bache M and Magatti D 2006 *J. Mod. Opt.* **53** 739
- [3] Valencia A, Scarcelli G and D' Angelo M 2005 *Phys. Rev. Lett.* **94** 063601
- [4] Gatti A, Magatti D and Bache M 2005 *Phys. Rev. Lett.* **94** 183602
- [5] Basano L and Ottonello P 2006 *Appl. Phys. Lett.* **89** 091109
- [6] Erkmen B I and Shapiro J H 2008 *Phys. Rev. A* **77** 043809
- [7] Erkmen B I and Shapiro J H 2009 *Phys. Rev. A* **79** 023833
- [8] Bromberg Y, Katz O and Silberberg Y 2009 *Phys. Rev. A* **79** 053840
- [9] Hardy N D and Shapiro J H 2011 *Phys. Rev. A* **84** 063824
- [10] Cheng J 2009 *Opt. Express* **17** 7916
- [11] Shi D, Fan C and Zhang P 2013 *Opt. Express* **21** 2050
- [12] Chan K W, O'Sullivan M N and Boyd R W 2009 *Phys. Rev. A* **79** 033808
- [13] Duan D and Xia Y 2014 *J. Opt. Soc. Am.* **31** 183
- [14] Li L Z, Yao X R and Liu X F 2014 *Acta Phys. Sin.* **63** 224201 (in Chinese)
- [15] Gong W, Zhao C and Jiao J 2013 arXiv:1301.5767 [quant-ph]
- [16] Hong Y, Li E R and Gong W L 2015 *Opt. Express* **23** 14541
- [17] Bache M, Brambilla E and Gatti A 2004 *Opt. Express* **12** 6067
- [18] Cheng J, Han S and Yan Y 2006 *Chin. Phys.* **15** 2002
- [19] Erkmen B I and Shapiro J H 2009 *Phys. Rev. A* **79** 023833
- [20] Hardy N D and Shapiro J H 2010 *SPIE Optical Engineering + Applications*, August 30, 2010, San Diego, California, USA, p. 78150L

Chinese Physics B

Volume 24

Number 12

December 2015

TOPICAL REVIEW — 8th IUPAP International Conference on Biological Physics

- 120201 Accurate treatments of electrostatics for computer simulations of biological systems: A brief survey of developments and existing problems**
Yi Sha-Sha, Pan Cong and Hu Zhong-Han
- 120504 Computational studies on the interactions of nanomaterials with proteins and their impacts**
An De-Yi, Su Ji-Guo, Li Chun-Hua and Li Jing-Yuan
- 126101 Structural modeling of proteins by integrating small-angle x-ray scattering data**
Zhang Yong-Hui, Peng Jun-Hui and Zhang Zhi-Yong
- 128701 Knowledge-based potentials in bioinformatics: From a physicist's viewpoint**
Zheng Wei-Mou
- 128702 A multi-field approach to DNA condensation**
Ran Shi-Yong and Jia Jun-Li
- 128703 Theoretical studies on sRNA-mediated regulation in bacteria**
Chang Xiao-Xue, Xu Liu-Fang and Shi Hua-Lin
- 128707 Application of self-consistent field theory to self-assembled bilayer membranes**
Zhang Ping-Wen and Shi An-Chang
- 128709 Firing dynamics of an autaptic neuron**
Wang Heng-Tong and Chen Yong

SPECIAL TOPIC — 8th IUPAP International Conference on Biological Physics

- 120202 The construction of general basis functions in reweighting ensemble dynamics simulations: Reproduce equilibrium distribution in complex systems from multiple short simulation trajectories**
Zhang Chuan-Biao, Li Ming and Zhou Xin
- 120501 Langevin approach with rescaled noise for stochastic channel dynamics in Hodgkin–Huxley neurons**
Huang Yan-Dong, Li Xiang and Shuai Jian-Wei
- 126402 Saturated sodium chloride solution under an external static electric field: A molecular dynamics study**
Ren Gan and Wang Yan-Ting
- 127308 Colloidally deposited nanoparticle wires for biophysical detection**
Sophie C. Shen, Liu Wen-Tao and Diao Jia-Jie
- 128201 Label-free surface-enhanced infrared spectro-electro-chemical analysis of the Redox potential shift of cytochrome *c* complexed with a cardiolipin-containing lipid membrane of varied composition**
Liu Li, Wu Lie, Zeng Li and Jiang Xiu-E

(Continued on the Bookbinding Inside Back Cover)

128202 Computational prediction of over-annotated protein-coding genes in the genome of *Agrobacterium tumefaciens* strain C58

Yu Jia-Feng, Sui Tian-Xiang, Wang Hong-Mei, Wang Chun-Ling, Jing Li and Wang Ji-Hua

128704 Catch-bond behavior of DNA condensate under tension

Li Wei, Wong Wei-Juan, Lim Ci-Ji, Ju Hai-Peng, Li Ming, Yan Jie and Wang Peng-Ye

128705 Comparison of ligand migration and binding in heme proteins of the globin family

Karin Nienhaus and G. Ulrich Nienhaus

128708 One-dimensional chain of quantum molecule motors as a mathematical physics model for muscle fibers

Si Tie-Yan

TOPICAL REVIEW — Magnetism, magnetic materials, and interdisciplinary research

127504 Magnetocaloric effects in RTX intermetallic compounds ($R = \text{Gd-Tm}$, $T = \text{Fe-Cu}$ and Pd , $X = \text{Al}$ and Si)

Zhang Hu and Shen Bao-Gen

127505 Novel magnetic vortex nanorings/nanodiscs: Synthesis and theranostic applications

Liu Xiao-Li, Yang Yong, Wu Jian-Peng, Zhang Yi-Fan, Fan Hai-Ming and Ding Jun

127506 Self-assembled superparamagnetic nanoparticles as MRI contrast agents — A review

Su Hong-Ying, Wu Chang-Qiang, Li Dan-Yang and Ai Hua

128501 Real-space observation of individual skyrmions in helimagnetic nanostripes

Jin Chi-Ming and Du Hai-Feng

RAPID COMMUNICATION

126301 Raman phonons in multiferroic FeVO_4 crystals

Zhang An-Min, Liu Kai, Ji Jian-Ting, He Chang-Zhen, Tian Yong, Jin Feng and Zhang Qing-Ming

GENERAL

120301 Thermal vacuum state corresponding to squeezed chaotic light and its application

Wan Zhi-Long, Fan Hong-Yi and Wang Zhen

120302 Dynamics of super-quantum discord and direct control with weak measurement in open quantum system

Ji Ying-Hua

120303 Decoherence of genuine multipartite entanglement for local non-Markovian-Lorentzian reservoirs

Mazhar Ali

120304 Quantum speed limits for Bell-diagonal states

Han Wei, Jiang Ke-Xia, Zhang Ying-Jie and Xia Yun-Jie

120305 A note on local unitary equivalence of isotropic-like states

Zhang Ting-Gui, Hua Bo-Bo, Li Ming, Zhao Ming-Jing and Yang Hong

120306 Fast multi-copy entanglement purification with linear optics

Cai Chun, Zhou Lan and Sheng Yu-Bo

120307 Free-space measurement-device-independent quantum-key-distribution protocol using decoy states with orbital angular momentum

Wang Le, Zhao Sheng-Mei, Gong Long-Yan and Cheng Wei-Wen

120401 Unstable and exact periodic solutions of three-particles time-dependent FPU chains

Liu Qi-Huai, Xing Ming-Yan, Li Xin-Xiang and Wang Chao

120502 Composition and temperature dependences of site occupation for Al, Cr, W, and Nb in MoSi₂

Li Xiao-Ping, Sun Shun-Ping, Yu Yun, Wang Hong-Jin, Jiang Yong and Yi Dan-Qing

120503 Entransy analyses of heat–work conversion systems with inner irreversible thermodynamic cycles

Cheng Xue-Tao and Liang Xin-Gang

120601 Border effect-based precise measurement of any frequency signal

Bai Li-Na, Ye Bo, Xuan Mei-Na, Jin Yu-Zhen and Zhou Wei

120701 Multistability of delayed complex-valued recurrent neural networks with discontinuous real-imaginary-type activation functions

Huang Yu-Jiao and Hu Hai-Gen

ATOMIC AND MOLECULAR PHYSICS

123101 Influence of a strong magnetic field on the hydrogen molecular ion using B-spline-type basis-sets

Zhang Yue-Xia and Zhang Xiao-Long

123201 Comment on “Relativistic atomic data for W XLVII” by S. Aggarwal *et al.* [*Chin. Phys. B* 24 (2015) 053201]

Kanti M. Aggarwal

123401 Fast-electron-impact study on excitations of 4d electron of xenon

Zhang Xin, Liu Ya-Wei, Peng Yi-Geng, Xu Long-Quan, Ni Dong-Dong, Kang Xu, Wang Yang-Yang, Qi Yue-Ying and Zhu Lin-Fan

123601 Solvation of halogen ions in aqueous solutions at 500 K–600 K under 100 atm

Shen Hao, Hao Ting and Zhang Feng-Shou

ELECTROMAGNETISM, OPTICS, ACOUSTICS, HEAT TRANSFER, CLASSICAL MECHANICS, AND FLUID DYNAMICS

124101 Design of ultra wideband microwave absorber effectual for objects of arbitrary shape

Gong Yuan-Xun, Zhou Zhong-Xiang, Jiang Jian-Tang and Zhao Hong-Jie

124102 Propagation of an Airy–Gaussian beam in uniaxial crystals

Zhou Mei-Ling, Chen Chi-Dao, Chen Bo, Peng Xi, Peng Yu-Lian and Deng Dong-Mei

124201 Propagation of rotating elliptical Gaussian beams from right-handed material to left-handed material

Peng Xi, Chen Chi-Dao, Chen Bo and Deng Dong-Mei

124202 Increasing the range accuracy of three-dimensional ghost imaging lidar using optimum slicing number method

Yang Xu, Zhang Yong, Xu Lu, Yang Cheng-Hua, Wang Qiang, Liu Yue-Hao and Zhao Yuan

- 124203 Dynamical properties of total intensity fluctuation spectrum in two-mode Nd:YVO₄ microchip laser**
Zhang Shao-Hui, Zhang Shu-Lian, Tan Yi-Dong and Sun Li-Qun
- 124204 Yb-doped passively mode-locked fiber laser with Bi₂Te₃-deposited**
Li Lu, Yan Pei-Guang, Wang Yong-Gang, Duan Li-Na, Sun Hang and Si Jin-Hai
- 124205 Analytical model for thermal lensing and spherical aberration in diode side-pumped Nd:YAG laser rod having Gaussian pump profile**
M H Moghtader Dindarlu, M Kavosh Tehrani, H Saghafifar and A Maleki
- 124206 Effects of 946-nm thermal shift and broadening on Nd³⁺:YAG laser performance**
Seyed Ebrahim Pourmand and Ghasem Rezaei
- 124207 Photoluminescence characteristics of ZnTe bulk crystal and ZnTe epilayer grown on GaAs substrate by MOVPE**
Lü Hai-Yan, Mu Qi, Zhang Lei, Lü Yuan-Jie, Ji Zi-Wu, Feng Zhi-Hong, Xu Xian-Gang and Guo Qi-Xin
- 124208 Tunable negative-index photonic crystals using colloidal magnetic fluids**
Geng Tao, Wang Xin, Wang Yan and Dong Xiang-Mei
- 124209 Strictly non-blocking 4×4 silicon electro-optic switch matrix**
Zhou Pei-Ji, Xing Jie-Jiang, Li Xian-Yao, Li Zhi-Yong, Yu Jin-Zhong and Yu Yu-De
- 124301 Acoustic radiation from the submerged circular cylindrical shell treated with active constrained layer damping**
Yuan Li-Yun, Xiang Yu, Lu Jing and Jiang Hong-Hua
- 124302 Theoretical analysis of transcranial Hall-effect stimulation based on passive cable model**
Yuan Yi and Li Xiao-Li
- 124701 Application of Arnoldi method to boundary layer instability**
Zhang Yong-Ming and Luo Ji-Sheng
- PHYSICS OF GASES, PLASMAS, AND ELECTRIC DISCHARGES**
- 125201 Study of hysteresis behavior in reactive sputtering of cylindrical magnetron plasma**
H. Kakati and S. M. Borah
- 125202 A computational modeling study on the helium atmospheric pressure plasma needle discharge**
Qian Mu-Yang, Yang Cong-Ying, Liu San-Qiu, Wang Zhen-Dong, Lv Yan and Wang De-Zhen
- 125203 A two-dimensional model of He/O₂ atmospheric pressure plasma needle discharge**
Qian Mu-Yang, Yang Cong-Ying, Chen Xiao-Chang, Liu San-Qiu, Yan Wen, Liu Fu-Cheng and Wang De-Zhen
- CONDENSED MATTER: STRUCTURAL, MECHANICAL, AND THERMAL PROPERTIES**
- 126102 Relationship between Voronoi entropy and the viscosity of Zr₃₆Cu₆₄ alloy melt based on molecular dynamics**
Gao Wei, Feng Shi-Dong, Zhang Shi-Liang, Qi Li and Liu Ri-Ping
- 126103 Krypton ion irradiation-induced amorphization and nano-crystal formation in pyrochlore Lu₂Ti₂O₇ at room temperature**
Xie Qiu-Rong, Zhang Jian, Yin Dong-Min, Guo Qi-Xun and Li Ning

(Continued on the Bookbinding Inside Back Cover)

- 126104 Effect of combined platinum and electron on the temperature dependence of forward voltage in fast recovery diode**
Jia Yun-Peng, Zhao Bao, Yang Fei, Wu Yu, Zhou Xuan, Li Zhe and Tan Jian
- 126201 Electronic structures and magnetisms of the $\text{Co}_2\text{TiSb}_{1-x}\text{Sn}_x$ ($x = 0, 0.25, 0.5$) Heusler alloys: A theoretical study of the shape-memory behavior**
Wang Li-Ying, Dai Xue-Fang, Wang Xiao-Tian, Lin Ting-Ting, Chen Lei, Liu Ran, Cui Yu-Ting and Liu Guo-Dong
- 126302 Material properties dependent on the thermal transport in a cylindrical nanowire**
Zhang Yong, Xie Zhong-Xiang, Deng Yuan-Xiang, Yu Xia and Li Ke-Min
- 126401 Effects of temperature gradient on the interface microstructure and diffusion of diffusion couples: Phase-field simulation**
Li Yong-Sheng, Wu Xing-Chao, Liu Wei, Hou Zhi-Yuan and Mei Hao-Jie
- 126403 Multiple patterns of diblock copolymer confined in irregular geometries with soft surface**
Li Ying, Sun Min-Na, Zhang Jin-Jun, Pan Jun-Xing, Guo Yu-Qi, Wang Bao-Feng and Wu Hai-Shun
- 126701 Interfacial and electrical characteristics of a $\text{HfO}_2/\text{n-InAlAs}$ MOS-capacitor with different dielectric thicknesses**
Guan He, Lv Hong-Liang, Guo Hui, Zhang Yi-Men, Zhang Yu-Ming and Wu Li-Fan
- 126801 Electrical properties and microstructural characterization of Ni/Ta contacts to n-type 6H-SiC**
Zhou Tian-Yu, Liu Xue-Chao, Huang Wei, Zhuo Shi-Yi, Zheng Yan-Qing and Shi Er-Wei
- CONDENSED MATTER: ELECTRONIC STRUCTURE, ELECTRICAL, MAGNETIC, AND OPTICAL PROPERTIES**
- 127101 First-principles calculation of the electronic structure, chemical bonding, and thermodynamic properties of $\beta\text{-US}_2$**
Li Shi-Chang, Zheng Yuan-Lei, Ma Sheng-Gui, Gao Tao and Ao Bing-Yun
- 127301 Spin-valley quantum Hall phases in graphene**
Tian Hong-Yu
- 127302 Spoof surface plasmons resonance effect and tunable electric response of improved metamaterial in the terahertz regime**
Wang Yue, Zhang Li-Ying, Mei Jin-Shuo, Zhang Wen-Chao and Tong Yi-Jing
- 127303 Shape effects on the ground-state energy of a three-electron quantum dot**
Z. D. Vatansever, S. Sakiroglu and İ. Sokmen
- 127304 High- k gate dielectric GaAs MOS device with LaON as interlayer and NH_3 -plasma surface pretreatment**
Liu Chao-Wen, Xu Jing-Ping, Liu Lu and Lu Han-Han
- 127305 Influence of ultra-thin TiN thickness (1.4 nm and 2.4 nm) on positive bias temperature instability (PBTI) of high- k /metal gate nMOSFETs with gate-last process**
Qi Lu-Wei, Yang Hong, Ren Shang-Qing, Xu Ye-Feng, Luo Wei-Chun, Xu Hao, Wang Yan-Rong, Tang Bo, Wang Wen-Wu, Yan Jiang, Zhu Hui-Long, Zhao Chao, Chen Da-Peng and Ye Tian-Chun

(Continued on the Bookbinding Inside Back Cover)

- 127306 Investigation of trap states in Al₂O₃ InAlN/GaN metal–oxide–semiconductor high-electron-mobility transistors**
Zhang Peng, Zhao Sheng-Lei, Xue Jun-Shuai, Zhu Jie-Jie, Ma Xiao-Hua, Zhang Jin-Cheng and Hao Yue
- 127307 Structures and electrical properties of pure and vacancy-included ZnO NWs of different sizes**
Yu Xiao-Xia, Zhou Yan, Liu Jia, Jin Hai-Bo, Fang Xiao-Yong and Cao Mao-Sheng
- 127309 Multi-step shot noise spectrum induced by a local large spin**
Niu Peng-Bin, Shi Yun-Long, Sun Zhu and Nie Yi-Hang
- 127401 First-principles simulation of Raman spectra and structural properties of quartz up to 5 GPa**
Liu Lei, Lv Chao-Jia, Zhuang Chun-Qiang, Yi Li, Liu Hong and Du Jian-Guo
- 127402 Study of Nb/Nb_xSi_{1-x}/Nb Josephson junction arrays**
Cao Wen-Hui, Li Jin-Jin, Zhong Yuan and He Qing
- 127501 Observation of spin glass transition in spinel LiCoMnO₄**
Chen Hong, Yang Xu, Zhang Pei-Song, Liang Lei, Hong Yuan-Ze, Wei Ying-Jin, Chen Gang, Du Fei and Wang Chun-Zhong
- 127502 Structure, morphology, and magnetic properties of high-performance NiCuZn ferrite**
He Xue-Min, Yan Shi-Ming, Li Zhi-Wen, Zhang Xing, Song Xue-Yin, Qiao Wen, Zhong Wei and Du You-Wei
- 127503 Fabrication and magnetic properties of 4SC(NH₂)₂-Ni_{0.97}Cu_{0.03}Cl₂ single crystals**
Chen Li-Min, Guo Ying, Liu Xu-Guang, Xie Qi-Yun, Tao Zhi-Kuo, Chen Jing, Zhou Ling-Ling and Liu Chun-Sheng
- 127507 Al-doping-induced magnetocapacitance in the multiferroic AgCrS₂**
Liu Rong-Deng, He Lun-Hua, Yan Li-Qin, Wang Zhi-Cui, Sun Yang, Liu Yun-Tao, Chen Dong-Feng, Zhang Sen, Zhao Yong-Gang and Wang Fang-Wei
- 127508 Spin frustration and magnetic ordering in triangular lattice antiferromagnet Ca₃CoNb₂O₉**
Dai Jia, Zhou Ping, Wang Peng-Shuai, Pang Fei, Tim J. Munsie, Graeme M. Luke, Zhang Jin-Shan and Yu Wei-Qiang
- 127701 Multifold polar states in Zn-doped Sr_{0.9}Ba_{0.1}TiO₃ ceramics**
Guo Yan-Yan, Guo Yun-Jun, Wei Tong and Liu Jun-Ming
- 127702 First-principles study of the relaxor ferroelectricity of Ba(Zr, Ti)O₃**
Yang Li-Juan, Wu Ling-Zhi and Dong Shuai
- 127703 Comparative research on the optical properties of three surface patterning ZnO ordered arrays**
Hou Kai, Zhu Ya-Bin and Qiao Lu
- 127704 Ultrahigh frequency tunability of aperture-coupled microstrip antenna via electric-field tunable BST**
Du Hong-Lei, Xue Qian, Gao Xiao-Yang, Yao Feng-Rui, Lu Shi-Yang, Wang Ye-Long, Liu Chun-Heng, Zhang Yong-Cheng, Lü Yue-Guang and Li Shan-Dong
- 127801 Variation of efficiency droop with quantum well thickness in InGaN/GaN green light-emitting diode**
Liu Wei, Zhao De-Gang, Jiang De-Sheng, Chen Ping, Liu Zong-Shun, Zhu Jian-Jun, Li Xiang, Liang Feng, Liu Jian-Ping and Yang Hui

127802 Optical properties of F- and H-terminated armchair silicon nanoribbons

Lu Dao-Bang, Pu Chun-Ying, Song Yu-Ling, Pan Qun-Na, Zhou Da-Wei and Xu Hai-Ru

127803 Dielectric and magnetic properties of (Zn, Co) co-doped SnO₂ nanoparticles

Rajwali Khan and Fang Ming-Hu

INTERDISCIPLINARY PHYSICS AND RELATED AREAS OF SCIENCE AND TECHNOLOGY

128101 Charge trapping in surface accumulation layer of heavily doped junctionless nanowire transistors

Ma Liu-Hong, Han Wei-Hua, Wang Hao, Yang Xiang and Yang Fu-Hua

128401 Optimal satisfaction degree in energy harvesting cognitive radio networks

Li Zan, Liu Bo-Yang, Si Jiang-Bo and Zhou Fu-Hui

128706 Al-doping influence on crystal growth of Ni–Al alloy: Experimental testing of a theoretical model

Rong Xi-Ming, Chen Jun, Li Jing-Tian, Zhuang Jun and Ning Xi-Jing

128710 Energy dependence on the electric activities of a neuron

Song Xin-Lin, Jin Wu-Yin and Ma Jun

128711 Linear-fitting-based similarity coefficient map for tissue dissimilarity analysis in T_2^* -w magnetic resonance imaging

Yu Shao-De, Wu Shi-Bin, Wang Hao-Yu, Wei Xin-Hua, Chen Xin, Pan Wan-Long, Hu Jiani and Xie Yao-Qin

GEOPHYSICS, ASTRONOMY, AND ASTROPHYSICS

129501 Bayesian-MCMC-based parameter estimation of stealth aircraft RCS models

Xia Wei, Dai Xiao-Xia and Feng Yuan

JUST FOR AUTHORS
— CHINESE PHYSICS B